Diels Alder-mediated release of gemcitabine from hybrid nanoparticles for enhanced pancreatic cancer therapy

Adeolu Oluwasanmi, Wejdan Al-Shakarchi, Ayesha Manzur, Mohammed H. Aldebasi, Rayan S. Elsini, Malek K. Albusair, Katherine J. Haxton, Anthony D.M. Curtis, Clare Hoskins

PII: S0168-3659(17)30860-X
DOI: doi:10.1016/j.jconrel.2017.09.027
Reference: COREL 8970

To appear in: *Journal of Controlled Release*

Received date: 17 August 2017
Revised date: 13 September 2017
Accepted date: 18 September 2017

Please cite this article as: Adeolu Oluwasanmi, Wejdan Al-Shakarchi, Ayesha Manzur, Mohammed H. Aldebasi, Rayan S. Elsini, Malek K. Albusair, Katherine J. Haxton, Anthony D.M. Curtis, Clare Hoskins , Diels Alder-mediated release of gemcitabine from hybrid nanoparticles for enhanced pancreatic cancer therapy. The address for the corresponding author was captured as affiliation for all authors. Please check if appropriate. Corel(2017), doi:10.1016/j.jconrel.2017.09.027

Diels Alder-mediated release of gemcitabine from hybrid nanoparticles for enhanced pancreatic cancer therapy

Adeolu Oluwasanmi[a], Wejdan Al-Shakarchi[a], Ayesha Manzur[a], Mohammed H Aldebasi[b], Rayan S Elsini[b], Malek K Albusair[b], Katherine J Haxton[c], Anthony DM Curtis[a], Clare Hoskins[a*]

[a]Institute of Science and Technology in Medicine, School of Pharmacy, Keele University, Keele, ST5 5BG, UK

[b]College of Medicine, Al Imam Mohammad Ibn, Saud Islamic University, Riyadh, Saudi Arabia

[c]School of Physical and Geographical Sciences, Faculty of Natural Sciences, Keele University, Keele, ST5 5BG, UK

*Corresponding author: Dr Clare Hoskins, c.hoskins@keele.ac.uk , +441782 734799

Abstract

Hybrid nanoparticles (HNPs) have shown huge potential as drug delivery vehicles for pancreatic cancer. Currently, the first line treatment, gemcitabine, is only effective in 23.8% of patients. To improve this, a thermally activated system was developed by introducing a linker between HNPs and gemcitabine. Whereby, heat generation resulting from laser irradiation of the HNPs promoted linker breakdown resulting in prodrug liberation. *In vitro* evaluation in pancreatic adenocarcinoma cells, showed the prodrug was 4.3 times less cytotoxic than gemcitabine, but exhibited 11-fold improvement in cellular uptake. Heat activation of the formulation led to a 56% rise in cytotoxicity causing it to outperform gemcitabine by 26%. *In vivo* the formulation outperformed free gemcitabine with a 62% reduction in tumor weight in pancreatic xenografts. This HNP formulation is the first of its kind and has displayed superior anti-cancer activity as compared to the current first line drug gemcitabine after heat mediated controlled release.

Keywords: Pancreatic cancer, Gemcitabine, Hybrid nanoparticle, Thermo-responsive drug delivery, Diels Alder

Introduction

Pancreatic cancer has a 5-year survival rate after diagnosis of 3.7 % [1-3]. This particularly deadly type of cancer has the worst prognosis of all cancer types [4-6]. It is the 5th most common cause of cancer death in the UK [7] and 4th most common in the US [8,9]. It occurs in only 2.6 % of all cancer cases as of 2011, but is responsible for 5.2 % of cancer deaths in the UK, which is a significantly disproportionate survival statistic owing to its poor prognosis. Its 5-year survival rate has only increased from 2 % to 3.7 % on average since 1975. These statistics show the deadliness and great importance in improving the survival rates of those who are diagnosed with pancreatic cancer. Surgery is the only method capable of curing pancreatic cancer and is often accompanied by post-operative chemotherapy to reduce the chances of recurrence [10]. Even after early detection, subsequent surgery and post-operation chemotherapy the survival rate only increases to 21 % [4,10]. A contributing reason for this is because pancreatic cancer rarely causes noticeable symptoms primarily attributed to cancer until it is fairly advanced and has spread to surrounding tissues [11]. Once this has occurred, surgery is no longer an option and patient quality of life becomes the top priority [12].

In most cases of pancreatic cancer, gemcitabine (GEM) is given as a first line chemotherapy because it demonstrates therapeutic efficacy in halting tumor growth [13]. Even with the increased survival rate with GEM the prognosis for pancreatic cancer is still abysmal, as such urgent improvements and novel strategies in pancreatic cancer chemotherapeutics are needed. GEM has a response rate of 23.8 % which means that 76.2 % of patients taking GEM see no viable response to the drug [14,15]. GEM is an aggressively toxic compound which indiscriminately targets both cancerous and non-cancerous cells leading to the side effects associated with chemotherapy such as hair loss, nausea and fatigue [8,16]. It possesses low efficacy meaning that most of the drug is metabolised and excreted before being able to carry out its intended pharmaceutical activity. Even with significant cytotoxic effects, its dosage must be as high as possible to ensure that enough pharmaceutical activity at the site of action occurs, due to its poor biocompatibility. Its small molecular weight contributes to its rapid renal clearance. Combating this clinically involves providing frequent high doses of the drug which can cause hepatic and renal toxicity [17]. In order to improve patient outcomes, three major issues need to be addressed. These are: 1) lack of early diagnosis and lag time before treatment, 2) lack of drug permeability through the dense stroma in these tumors and 3) lack of drug specificity. This work aims to overcome these challenges by the development of nanoparticles with the capability for image guidance, targeting, deep penetration, and controllable drug release. Development of such platforms will form rapid and effective treatments which will result in improved patient prognosis.

Using model drug molecules, we have shown that after either incorporation onto / into nanoparticles [19,20], or drug encapsulation into polymeric micelles [21], consistently increased drug uptake is achieved *in vitro* in pancreatic cancer cells. Additionally, *in vivo* in pancreatic xenograft models, we have shown that after delivery in a nanoparticle formulation, drug molecules are significantly more capable of tumor retardation compared with free drug molecules [14].

Nano-sized formulations of cytotoxic agents have been proven to passively target cancerous tissue and promote increased drug efficacy via the enhanced permeability and retention effect (EPR). However, pancreatic adenocarcinoma is characterised by dense solid tumours, which reportedly do not allow for EPR accumulation [22-24]. As such, other mechanisms of drug targeting to the site of action such as active targeting with site specific ligands or local administration must be considered.

We have fabricated HNPs and demonstrated their potential for imaging using magnetic resonance imaging [25], heating after laser irradiation (by exploitation of surface plasmon resonance) in phantoms that mimic biological systems [26], *in vitro* [27] and *in vivo* [19]. We have also reported the use of these HNPs as drug carrier vehicles [28] and have demonstrated their utility as heat initiated drug release vehicles [19]. These systems confer highly controllable drug delivery and can be utilised in image guided stimuli-responsive drug delivery or used as theranostic agents. Recently, the use of HNPs as heat triggered vehicles for drug delivery by exploiting reversible electrostatic binding of charged drug molecules onto the surface of the hybrid nanoparticles was reported [19]. The study trialled novel bisnaphthalamide based drug compounds which had shown previous potential in cancer therapy. Significant drug release was observed at temperatures above 44 ˚C. *In vivo* evaluation after intra-tumoral (I.T.) administration to pancreatic xenograft models in nude mice resulted in 5-fold tumor retardation after heat initiation promoting drug release [19].

Recently, a growing trend in cancer therapeutics is to try and overcome side effects associated with systemic therapies. For many drug molecules and nanotechnology in specific, the main problem is the accumulation in the liver after IV administration and associated metabolic breakdown. Hence, a growing trend is to directly administer these potent compounds directly to the tumor site (I.T.). In fact, in 2017 reports have shown that nanoparticles [19, 29], microparticles [30], and peptides [31] have been all been administered *via* this route with a clinical trial in pancreatic cancer being outlined by Hajda *et al.* [32]. Multiple studies have been reported for the use of laser activated systems for either triggered drug release or for ablation in cancer therapy [19,33,34]. For the most, these systems rely on the use of minimally invasive surgery in order for the laser to access its destination due to limited penetration depths. Here, we proposed an I.T. administered formulation which then undergoes laser activation. Hence, since laser irradiation requires minimally invasive surgery, I.T. injection will be appropriate. In the case of pancreatic cancer, the patient prognosis is so bad that minimally invasive surgery is a viable option in order to prolong life.

This study aims to conjugate GEM onto the surface of HNPs in order to determine whether such coupling could increase drug efficacy in the solid tumors formed *in vivo*. Unfortunately, the physicochemical properties of GEM do not allow for electrostatic interaction with the HNP surface. As such a Diels Alder linker will be employed to conjugate the drug molecules onto the surface (Figure 1). By exploiting the thermal reversibility of Diels Alder cycloadducts, the thermal release of drug compounds can be initiated due to heat generation after laser irradiation of the HNPs *via* the surface plasmon resonance. Here we report the synthesis and evaluation of HNP-L-GEM both *in vitro* and *in vivo* for use as a heat triggered carrier for the precision treatment of pancreatic cancer.

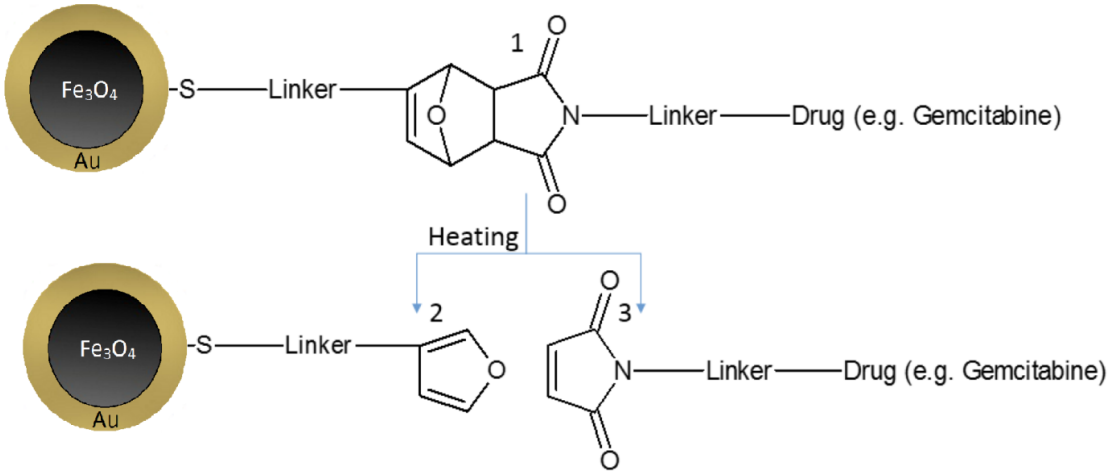

Figure 1. *Schematic representation of mechanism of drug loading/release from the hybrid nanoparticle surface via heat initiated reversal of the Diels Alder reaction.*

Methods

All chemicals were purchased from Alfa Aesar, UK unless otherwise stated and were at least ACS reagent grade or greater purity. Gemcitabine was purchased from Fluorochem, UK and was analytically pure. HPLC grade organic solvents used for chemical synthesis and analysis were purchased from Fisher Scientific, UK. Deuterated solvents were purchased from Cambridge Isotope Laboratories, USA. Visking membrane was purchased from Medicell, UK. Human pancreatic adenocarcinoma (BxPC-3) cells were purchased from ATCC, USA. Cell culture media and consumables were purchased from Fisher Scientific, UK.

Synthesis of L-GEM

^{1}H NMR spectra were recorded at 300 MHz using a Bruker Spectrospin DPX 300 Spectrometer. All NMR samples were made up in deuterated solvents with all values quoted in ppm relative to tetramethylsilane (TMS) as an internal reference. Coupling constants (*J* values) are reported in Hertz (Hz).

Maleic anhydride (0.98 g, 10 mmol) was dissolved in glacial acetic acid (20 mL) followed by γ-aminobutyric acid (1.03 g, 10 mmol). The mixture was vigorously stirred resulting in a slurry, which was stirred for a further 8 h at room temperature under a N_2 atmosphere. The white precipitate was collected by filtration and washed with water (20 mL × 2). The white solid was then dispersed in 20 mL of water and refluxed at 110 °C. Once a clear solution had formed, the mixture was further refluxed for an additional 30 min. The solution was left to cool before the water was evaporated off. A white precipitate formed which was filtered and washed with chilled water. The resultant white powder was then dried *in vacuo*. 4-maleimidobutyric acid [Compound 1] was obtained as a white powder (1.72 g, 94 % yield) [35]. Compound 1 ^{1}H NMR (SI-Figure 1): 6.03 (singlet, [5, 6] 2H), 2.81 (triplet, [4], 2H), 2.33 (triplet, J=7.3Hz [3], 2H), 1.74 (quintet, J=7.4Hz [2], 2H).

Di-*tert*-butyl dicarbonate (4.36 g, 20 mmol) was dissolved in 1,4 dioxane (40 mL) and the solution added dropwise to a stirred solution of gemcitabine hydrochloride (0.60 g, 2 mmol) in 1M aqueous potassium hydroxide (40 mL) over a period of 10 min. The mixture was stirred for 40 min at room temperature and monitored closely using thin-layer chromatography (TLC). After TLC confirmed the presence of a 50:50 mixture of the desired product with 3′-*O*-bis (*tert*-butoxycarbonyl) gemcitabine, the reaction mixture was extracted with ethyl acetate (80 mL × 3), the organic extracts washed with brine (20 mL × 2) and dried over magnesium sulfate. The mixture was then filtered and the filtrate was evaporated *in vacuo* to give a clear oily residue. The residue was dissolved in 1,4 dioxane (40 mL) and a solution of di-*tert*-butyl dicarbonate (4.36 g, 20 mmol) in 1M aqueous potassium hydroxide (40 mL). The mixture was stirred at room temperature and monitored by TLC. After TLC analysis confirmed that all 3′-*O*-bis(*tert*-butoxycarbonyl)gemcitabine had been consumed the reaction mixture was extracted with ethyl acetate (80 mL × 3), combined, washed with brine (20 mL × 2) and dried over magnesium sulfate. The mixture was then filtered and the filtrate was evaporated *in vacuo* to give a pale yellow oily residue. 3′,5′-*O*-Bis(*tert*-butoxycarbonyl)gemcitabine [Compound 2] was obtained as a colourless solid (0.326g, 63 %) after column chromatography using a 1:1 mixture of acetone:dichloromethane as eluent [36]. Compound 2 ^{1}H NMR (SI-Figure 2): 7.61 (doublet J=7.5Hz [6], 1H), 6.35 (doublet [7], 1H), 5.95 (singlet J=7.5Hz [5] 1H), 5.3 (singlet [4], 1H), 4.52, 4.46 (multiplet [3], 2H), 4.42 (doublet [2], 1H), 1.5 (singlet [9], 9H), 1.48 (singlet [8], 9H).

Maleic anhydride (2.9 g, 29 mmol) was dissolved in anhydrous dimethylformamide (35 mL). 4-aminobutyric acid (2.68 g, 26 mmol) was added to the solution and the mixture was stirred under an argon atmosphere at room temperature. After 3 h the mixture was cooled to 0 °C for 0.5 h. N-hydroxysuccinimide (3.7 g, 32 mmol) and 1-ethyl-3-(3-dimethylaminopropyl)-carbodiimide (11 g, 71 mmol) were added to the mixture. The mixture was stirred at 0 °C for 30 min before being allowed to warm to room temperature. The mixture was then stirred overnight at room temperature. The solvent was evaporated and the residue was dissolved in chloroform (300 mL). The organic solution was washed with saturated sodium bicarbonate (100 mL) and dried over magnesium sulfate. The mixture was filtered and the filtrate was evaporated to yield a dark green film. The N-hydroxysuccinimide ester of 4-aminobutyric acid [Compound 3] was obtained as a colourless powder (4.8 g, 66 %) after column chromatography using a 10:1 mixture of chloroform:methanol as eluent [35]. Compound 3 ^{1}H NMR (SI-Figure 3): 7.01 (singlet [6, 7], 2H), 3.48 (triplet J=7.0Hz [2], 2H), 2.80 (singlet [4, 5], 4H), 2.72 (triplet J=7.4Hz [3] 2H), 1.83 (quintet J=7.2Hz [1] 2H).

2-Furanmethane thiol (1.00 g, 8.9 mmol) and di-*tert*-butyl dicarbonate (1.80 g, 8.9 mmol) were dissolved in anhydrous acetonitrile (35 mL). Anhydrous potassium carbonate (2.4 g, 17.5 mmol) was added and the mixture was stirred at room temperature for 24 h under a N_2 atmosphere. The mixture was diluted with ethyl acetate (200 mL) and filtered with the aid of celite. The filtrate was washed with saturated sodium bicarbonate solution (40 mL) and dried over magnesium sulfate. The mixture was filtered and the filtrate was evaporated to give *O*-*tert*-butyl-*S*-(furan-2-ylmethyl)carbonothionate [Compound 4] as a brown oil (1.76 g, 93 %) [37]. Compound 4 ^{1}H NMR (SI-Figure 4): 7.34 (multiplet [3], 1H), 6.3 (multiplet [1], 1H), 6.23 (multiplet J=3.2Hz [2], 1H), 4.06 (singlet [4] 2H), 1.5 (singlet [5] 9H).

O-tert-butyl-*S*-(furan-2-ylmethyl)carbonothionate [Compound 4] (1.5 g, 9 mmol) was added into a sealed tube followed by diethyl ether (35 mL). The N-hydroxysuccinimide ester of 4-aminobutyric acid [Compound 3] (2.4 g, 9 mmol) was added and the mixture was stirred at room temperature for 7 days under a N_2 atmosphere. The protected cycloadduct [Compound 5] was obtained as a brown solid (2.14 g, 48.3 % yield) after column chromatography using a 1:1 mixture of petroleum ether (bpt 40-60 °C): ethyl acetate as eluent. Compound 5 ^{1}H NMR (SI-Figure 5): 6.53 (multiplet [4-endo], 1H), 6.41 (multiplet J=3.2Hz [4-exo], 1H), 6.31 (multiplet [3-endo] 1H), 6.24 (multiplet [3-exo] 1H), 5.24 (doublet J=1.7Hz [2], 1H), 4.06 (singlet [11] 2H), 3.61 (triplet [7], 2H), 3.59 (multiplet J=6.2Hz [1-endo], 1H), 3.44 (doublet J=6.2Hz [5-endo], 1H), 3.01 (singlet [1-exo] 1H), 2.95 (doublet [5-exo] 1H), 2.84 (singlet [9,10] 4H), 2.64 (triplet [8], 2H), 2.01 (quintet [6], 2H), 1.5 (singlet [12], 9H).

The cycloadduct [Compound 5] (3.94 g, 8.2 mmol) was dissolved in dry dichloromethane (30 mL). 3′, 5′-*O*-Bis-(*tert*-butoxycarbonyl) gemcitabine [Compound 2] (3.821 g, 8.2 mmol) was added to the stirred solution followed by diisopropylethylamine (5.82 mL, 41 mmol). The reaction mixture was stirred at 0 °C for 108 h under an argon atmosphere. The solvent was removed under reduced pressure to give a dark orange residue. Protected L-GEM [Compound 6] was obtained as a pale green powder (4.31 g, 62 % yield) after column chromatography using a mixture of 10:1 chloroform:methanol as eluent. Compound 6 ^{1}H NMR (SI-Figure 6): 7.89 (singlet [14], 1H), 7.29 (doublet J=7.2Hz [13], 1H), 6.48 (br-singlet [5-*endo*], 1H), 6.41 (br-singlet J=3.2Hz [5-*exo*], 1H), 6.27 (doublet J=4.2Hz [4-*endo*] 1H), 6.24 (multiplet [17] 1H), 6.16 (multiplet [4-*exo*] 1H), 5.5 (br-singlet [3-*endo*], 1H), 5.20 (br-singlet [12], 1H), 5.0 (br-singlet [3-*exo*], 1H), 4.45-4.31 (multiplet [10,11] 3H), 3.44 (triplet J=14.3Hz [8], 2H), 3.40 (br-singlet [2-*endo*], 1H), 3.29 (doublet J=14.5Hz [6-*endo*], H), 2.97 (br-singlet [2-*exo*], 1H) 2.89 (doublet J=6.4Hz [6-*exo*], 1H), 2.44 (triplet [9] 2H), 1.78 (triplet [7] 2H), 1.35 (doublet [16,18,19] 27H).

Protected L-GEM [Compound 6] (4.31 g, 5.1 mmol) was dissolved in 185 mL of a solution of 15 % trifluoroacetic acid in dichloromethane (v/v) and the solution stirred at 0 °C for 2 h. The volatile solvents were removed under reduced pressure to give a dark red residue. L-GEM [Compound 7] was isolated as a pale orange powder (1.3 g, 47 % yield) after column chromatography using a 1:1 mixture of acetone:dichloromethane as eluent. High resolution mass spectrometry of L-GEM was performed using a ThermoFisher Scientific LTQ Orbitrap XL hybrid ion trap-orbitrap mass spectrometer. Samples were introduced to the spectrometer as solutions in dichloromethane/methanol with ammonium acetate added. All compounds analysed gave satisfactory data at high resolution as compared to predicted ionisation patterns. FTIR analysis was carried out using a Thermo Scientific Nicolet™ IS5 FTIR fitted with an attenuated total reflectance adapter (Thermofisher, UK). A background correction scan was carried out prior to sample analysis. A series of 64 scans (resolution = 4nm) were carried out and an average deduced.

Retro Diels Alder linker breakdown at elevated temperatures

The linker was heated in deuterated acetone in a round bottom flask at various temperatures. A 2 mL sample of the reaction mixture was added to a NMR tube, sealed with parafilm and cooled down by immersion into ice cold water for 5 min.

The samples were then analysed with ^{1}H NMR spectroscopy (Bruker Avance 300 MHz NMR Spectrometer, Bruker, Germany). Aliquot samples were analysed at the 0, 5, 10, 15, 30, 60, 120 and 180 min mark and multiple round bottom flasks of the reaction mixture were heated to 37 °C, 45 °C and 70 °C in triplicate.

Synthesis and characterization of hybrid nanoparticles (HNPs)

Hybrid nanoparticle synthesis was carried out as previously reported [25,28,38]. Particles were analysed for their surface charge using a Malvern Zetasizer Nano ZS. The samples were analysed over 100 runs at 25 °C. TEM imaging was carried out using the JEOL JEM-1230 (JEOL, Japan) transmission electron microscope. Prior to imaging, formvar coated copper grids were prepared. The samples were pipetted (10 µL) onto the grids and allowed to air dry before imaging. Inductively Coupled Plasma – Optical Emission Spectroscopy (ICP-OES) was used to measure the metal content of the HNPs. Samples were prepared first by adding 0.4 mL of suspended nanoparticles to a 2 mL solution of 1:1 hydrochloric acid/nitric acid (1:5 dilution of 0.4 mL nanoparticles) which was gently heated for a few min until the nanoparticles were dissolved. The solutions were diluted in deionised water and analysed by an Agilent Technologies 700 series ICP-OES. The samples were compared to standard solutions in a calibration curve of Fe at 261.187 nm (R^2 = 0.9997) and Au at 242.794 nm (R^2 = 0.9981) for gold. Uv-Vis spectroscopy characterization of HNPs was carried out using a Varian Cary 50 Bio Uv-Vis spectrophotometer over a wavelength range of 400-700 nm in order to determine the maximum absorbance of the HNPs within this range.

Preparation of HNP-L-GEM

Into a sample tube, 5 mg of HNPs (based on iron mass) was added followed by 25 mg (based on gemcitabine mass) of the thiolated thermally labile drug (L-GEM). The mixture was diluted to 5 mL with deionised water and stirred for 2 h at room temperature. The HNP-L-GEM were magnetically separated and washed with 5 mL of deionised water. Total drug conjugation concentration was analysed using reverse phase HPLC. The peak area was used to calculate drug content from a calibration curve (R^2 = 0.999). The HPLC system coupled to a UV detector used was a Perkin Elmer, Flexar LC, Autosampler using a Pinnacle DB C18 reverse phase column. The flow rate for the solvent phase solution was 1 mL min^{-1} (1:1 v/v water:acetonitrile) for all samples unless otherwise stated and the sample injection amount is 10 µL. Sample fractions were analysed at 268 nm.

***In vitro* drug release studies**

A dialysis membrane (12-14 kDa) was filled with 2 mL of HNP-L-GEM. The membrane was placed into 200 mL water or cell media at varied pH (7.4, 5.6) under *sink* conditions. The solutions were stirred and the rate of drug release measured at varied temperatures (20 ˚C, 37 ˚C & 44 ˚C). Aliquots (1 mL) of the solution were taken at various time points (1 min, 2 min, 5 min, 10 min, 15 min, 30 min, 1 h, 2 h, 3 h, 4 h, 24 h, 48 h, 72 h and 96 h) and placed in HPLC vials. Fresh 1 mL of deionised water/cell culture media of appropriate pH was placed back into the conical flask. Total drug release was analysed using HPLC as described previously. Experiments were carried out in triplicate.

Stability assessment of formulation

Vials containing HNP-L-GEM were stored at room temperature away from direct sunlight or refrigerated. Every seven days over a four-week period, the particulate formulations were magnetically separated from solution and a 0.1 mL aliquot from the supernatant of each vial was analysed using HPLC to calculate the amount of GEM that had released from the HNP surface. HPLC was performed as previously described. Experiments were carried out in triplicate.

***In vitro* evaluation**

All *in vitro* experiments and results discussed in this study were carried out using the BxPC-3 cells. Well plate cell cultures were produced by seeding BxPC-3 cells in their exponential growth phase and allowing them to incubate overnight at 37 °C within a 5 % CO_2 atmosphere in RPMI-1640 media supplemented with a 1 % streptomycin penicillin and 5 % foetal bovine serum [39].

Cytotoxicity measurement

MTT assay

A 96-well plate was seeded with 15,000 of BxPC-3 cells/well and incubated for 24 h. The media was removed and the well plates were dosed with HNPs, GEM, gemcitabine prodrug with the maleimide residue of the linker attached indicating where linker breakdown has occurred but linker has not dissociated from parent drug molecule (Mal-GEM), HNP-L-GEM (0.01 μg mL^{-1} – 100 μg mL^{-1}), as well as mercaptofuran and HNP-mercaptofuran at the relative concentration on the particle surface (0.0042 μg mL^{-1} – 42 μg mL^{-1}) in order to indicate toxicity after drug release had occurred. All samples were diluted in cell culture media containing 10% FBS and incubated for 24 h, 48 h or 72 h. Following this, the media and PBS was removed and replaced with a 175 μL solution of 10 % MTT in media. The plate was then incubated for 4 h, afterwards, the media was removed and 175 μL of DMSO was added. The UV absorbance of the plate was analysed at 570 nm using a Tecan Infinite M200 Pro Microplate Reader. Percentage cell viability was calculated in respect to positive and negative controls. Experiments were conducted in triplicates.

Trypan blue exclusion assay

Cells were seeded into a 12-well plate at 25,000 cells/well. The plate was incubated for 24 h. The media was removed and the BxPC-3 cells dosed with HNP, GEM, Mal-GEM or HNP-L-GEM diluted in cell culture media containing 10% FBS (0.01 μg mL^{-1} – 100 μg mL^{-1}). The plate was incubated for 24 h, 48 h or 72 h. Afterwards, the wells were washed three times with PBS and the cells were trypsinized (75 μL) and suspended in 0.5 mL of media [40]. Into a fresh Eppendorf tube 75 μL of trypan blue and 75 μL aliquot of cell suspension was added. The cells were counted using a Countess Invitrogen Automated Cell Counter (Invitrogen, UK) and the live cell counts were compared to those of the control to produce a percentage cell viability value for each sample concentration. Experiments were conducted in triplicate.

Intracellular drug uptake

Cells were seeded into 6-well plates at 50,000 cells/well. The plates were incubated for 24 h before media was removed. Cells were dosed with 50 μg mL^{-1} solution of HNP, GEM, Mal-Gem or HNP-L-GEM diluted in cell culture media containing 10% FBS. The cells were incubated for 1 h, 4 h or 24 h. Following this, the cell media was removed and the wells were washed three times with PBS. The cells were suspended

with 185 mL of trypsin before 0.815 mL of the media was added. The cells were then counted and 100,000 cells were placed into an Eppendorf tube. Deionised water was then added until the total volume of each tube was 1 mL. Centrifugation of this solution in a Hermule Z-323 centrifuge at 500 rpm for 5 min, drives the cell fragments to the bottom of the Eppendorf tube. The supernatant was removed and analysed *via* HPLC to determine drug content as previously described. The drug weight per cell was calculated. The experiment was carried out in triplicate.

Effect of heat on cell viability

The trypan blue assay was repeated with one alteration in method. After the cells had been dosed with the relevant formulation the incubation temperature was raised to 44 °C over a period of 0.5 h in order for bulk solution to equilibrate (measured using thin wired thermocouples in a control well). The temperature was held at 44 °C for 30 sec, before returning back into the 37 °C, 50 % CO_2 incubator [19]. The plates were further incubated for 48 h. The IC_{50} was determined for all 6 plates and the heat activated IC_{50} results were compared to the non-activated plates to note the effect on percentage cell viability. The experiments were carried out in triplicate.

***In vivo* evaluation**

Female Nu/Nu mice, 4-5 wks old (Charles River, UK) were housed in pathogen-free conditions (weight of mice was 20–30 g). All procedures and animal care were carried out according to Project License PPL 70/8806 granted by the UK Home Office.

Dose tolerability

Healthy mice were injected intraperitoneal with HNPs (25 mg Kg^{-1}) and Mal-GEM (6 mg Kg^{-1}) (n=2) once per week for 4 weeks. Mouse weight was recorded daily and monitored over the duration of the study as an indication of gross toxicity.

Therapeutic Study

Human pancreatic cancer cell line BxPC-3 was cultured to 90 % confluence in RPMI 1640 media supplemented with 10 % fetal bovine serum and 1 % penicillin streptomycin. The cells were washed in PBS and trypsinized. The cells were washed with PBS, centrifuged at 800 rpm for 5 min and resuspended in 50:50 serum free media:PBS. The tumor cell suspension (3.0 X 10^6 cells in 100 μL) was injected subcutaneously (s.c.) in the right flank of each mouse. When the tumor became palpable, measurements in two dimensions with vernier callipers were carried out twice a week and tumors volume calculated using $V = 4/3\pi[(D_1 + D_2)/4]^3$. Once tumors had reached 0.1 cm^3 therapeutic studies commenced. The mice were grouped into 8 arms (n=5) of control, HNP, GEM, HNP-L-GEM all with and without laser irradiation. Drug administration was given at 3 mg Kg^{-1} with equivalent HNP concentration used in the HNP control. Doses were injected I.T. using a 26-gauge needle (Vet-Tech, UK) at a maximum of 100 μL. The dose was administered one dose per wk over a 4 wk period. Where laser irradiation was required this was carried out 24 h after dosing under anaesthetic. The tumor was irradiated at 1064 nm for 20 sec using a ML-LASER-YB5 Q-switched Nd:YAG Laser Treatment System (WeiFang MingLiang Electronics Company Ltd., China). Pulse width: 10 ns, pulse repetition frequency: 6 Hz, laser spot diameter: 3 mm, cooling system: water cooled with airflow cooling. The beam was collimated through concave lenses to a 1 mm

diameter. Any mouse whose tumor volume reached 0.9 cm^3 was sacrificed in line with good practice guidelines [41].

Statistical analysis

A simple two tailed t-test was carried out to determine the statistical significance of results, whereby $p \leq 0.01$ was significant.

Results and Discussion

Synthesis of HNP-L-GEM

Attachment of the thermally labile linker onto the gemcitabine molecule was achieved according to the general scheme shown in Figure 2. The identity of the final compound (L-GEM) was confirmed by NMR spectroscopy, Mass spectrometry and Fourier transform infrared spectroscopy. (SI-Figure 7). Analysis of L-GEM indicated the complete boc deprotection of the thiol and hydroxyl groups. Coincidentally a very strong garlic odour was detected from the compound which is a common trait amongst thiol compounds [42]. The HNPs were successfully synthesized, analysis of their synthetic pathway can be observed in Figure 3. Attachment of L-GEM onto the HNP surface occurred by dative covalent binding between the thiol residue in the linker moiety with the gold surface of the HNPs. The HPLC data showed that the gemcitabine analogue binding occurred (5 mg GEM:1 mg HNP) with 98 % efficiency. We can estimate how many furan-maleimide cycloadducts have been conjugated onto the HNP surface (1.13×10^{19} molecules per mg Fe), and therefore, once 100% release has occurred we can quantify the exact exposure (which equates to 1.87×10^{-5} mol).

The furan moiety is found in many delivery systems described in the literature which are based around a reversible furan-maleimide Diels-Alder reaction, of which most are polymer based [43]. These usually contain many furan residues (often regarded as toxic) in the parent polymer that is being loaded with the maleimide-conjugated drug. Reports have documented that not all furan conjugation sites are occupied after drug loading leaving the furan exposed in its native form [44]. In our HNP system, the Diels-Alder linkage is produced before drug conjugation, hence, no furan excess is required. For these particles, this concentration is far lower than that of the reported polymers. These furans are conjugated onto the HNP *via* dative covalent binding, which will only breakdown at temperatures far above our target temperature. Hence, any metabolites produced will remain attached to the HNP and remain localised to the tumor.

Due to the high level of loading, it is likely that the HNP surface was not saturated and that higher loading quantities may have been achievable at higher drug:HNP feed ratios.

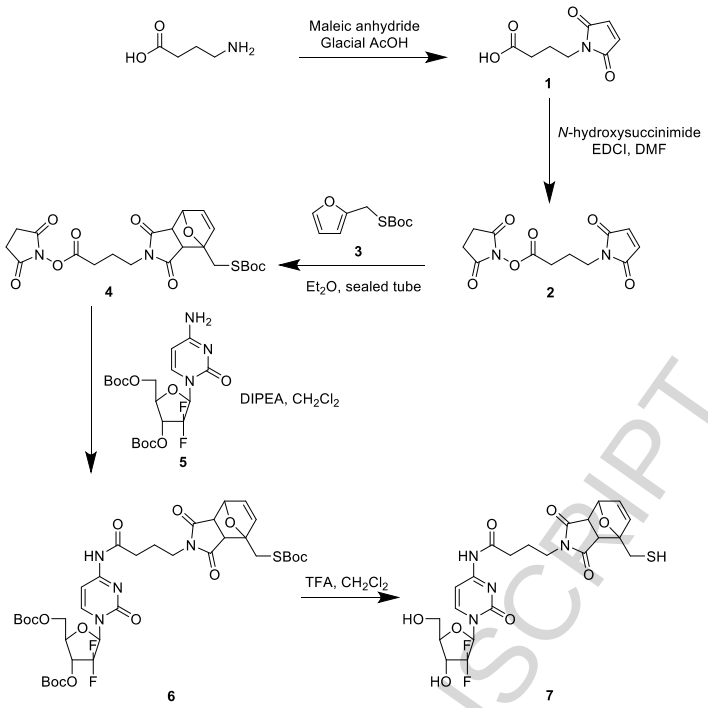

Figure 2. *Reaction scheme for the synthesis of the Diels Alder cycloadduct formation and conjugation onto gemcitabine forming L-GEM [Compound 7].*

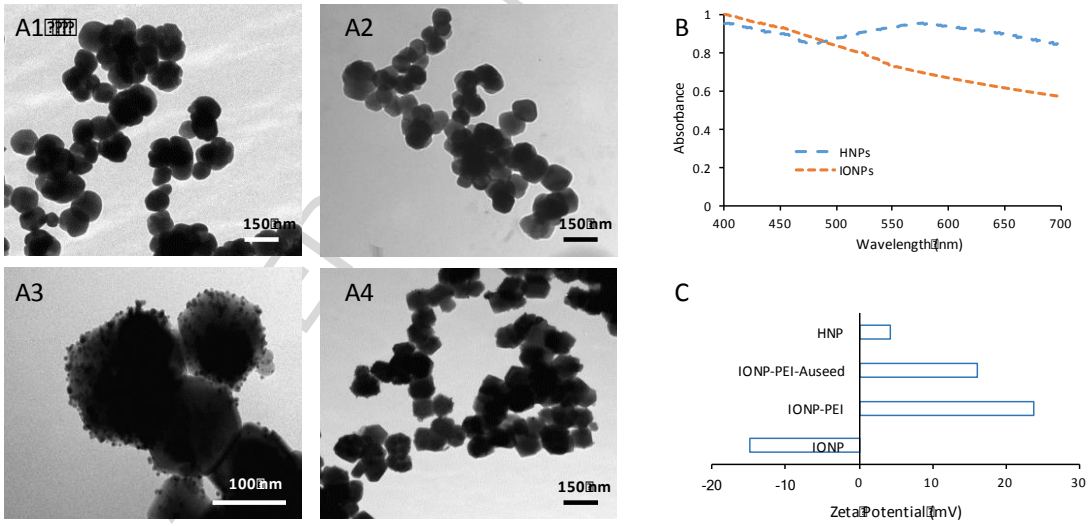

Figure 3. *Physical characterization of nanoparticles using A) TEM 1. Uncoated iron oxide, 2. PEI coated iron oxide, 3. Gold seeds attached to PEI coated iron oxide and 4. HNPs. B) UV-Vis spectroscopy scanning between 400 nm – 700 nm. C) Zeta potential measurement carried out in water at room temperature.*

In vitro drug release studies

Drug release occurs in this system when a threshold temperature is met or exceeded which is resultant from laser irradiation. Here we purposefully designed a system

which would release at approximately 44 ºC in order to allow drug release to occur below the temperatures which would result in cellular ablation.

The released drug compound will have a maleimide chain attached onto it, differing in structure to the native GEM molecule. Hence, the released compound will be called Mal-GEM. Drug release at increasing temperature was carried out at pH 7 (water), pH 5.6 (cell media) and pH 7.4 (cell media). The pH's were chosen due to their biological relevance. Figure 4A shows the percentage release of detected Mal-GEM over time from the HNP-L-GEM in water, pH 7. At 20 ˚C in there is negligible Mal-GEM release over the time period tested ($P < 0.05$).

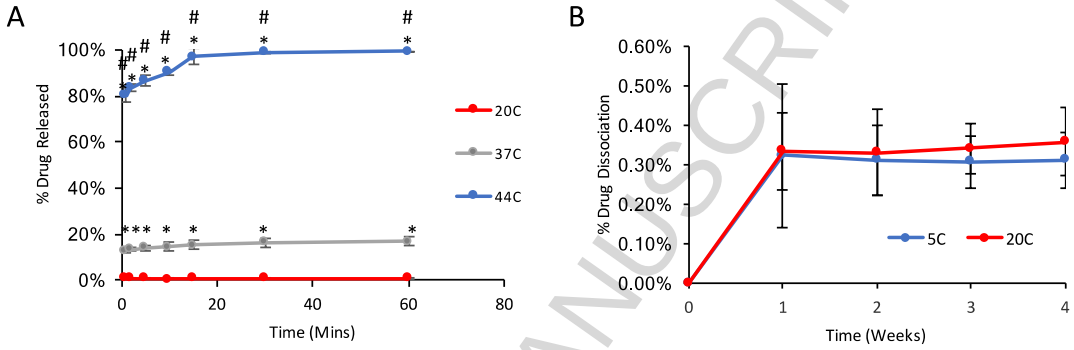

Figure 4. *Evaluation of HNP-L-GEM. A) In vitro drug release carried out at varied temperatures in water and B) Stability of formulation stored in the fridge and at room temperature over 4 weeks (n=3, ±SD). * denotes significance compared with 20 ºC and # compared with all other temperatures tested (p<0.01).*

This trend was also observed at pH 7.4 and pH 5.6 (SI-Figure 9). Drug release was also carried out at 37 °C in order to mimic what may happen at body temperature. At pH 7, the HNP-L-GEM formulation showed a time dependant release. There was an initial burst release where 13 % of the GEM was released within 60 sec, after which no further release was observed (Figure 4A). The initial burst release of Mal-GEM from HNP-L-GEM at pH 7.4 (SI-Figure 9A) and pH 5.6 (SI-Figure 9B) at 37 °C was 13 % and 14 % respectively. Mal-GEM release was analysed at 44 °C, this temperature was used to mimic the temperature of HNPs after laser irradiation. These studies were carried out at varied pH (7, 7.4, & 5.6 as previously discussed). Figure 4A confirms that at this elevated temperature, a rapid and significantly increased release of Mal-GEM from the HNP-L-GEM was observed. At pH 7, 80 % of the Mal-GEM had been released after only 60 sec. At a pH of 7.4 (SI-Figure 9A) 80 % of Mal-GEM was released with 81 % being released at pH 5.6 (SI-Figure 9B) after 60 sec.

This large increase in release rate is in agreement with in-depth modelling and experimental study into the kinetics of the Diels Alder reaction and the corresponding retro Diels Alder reaction of 2-substituted furans with N-alkylated maleimides [45]. Froidevaux *et al.* reported that for a 10 ºC increase in temperature they observed

almost a 5 x increase in the rate of the retro Diels Alder reaction, using cycloadducts similar to the one used in our linker [45].

Our findings confirm that temperature is the major factor which influences the induction of retro Diels Alder reaction and hence liberation of Mal-GEM molecules. Hence, these systems have potential as thermally triggered drug delivery vehicles

Stability assessment of formulation

The data in Figure 4B shows negligible drug dissociation at both 20 °C and 5 °C ($p < 0.01$). Hence, it can be deduced that storage of the formulations would result in stable systems over a 4-week period. In comparison with other **t**hermally responsive drug delivery systems for the transport and release of GEM this stability profile is exciting. The use of magnetoliposomes to encapsulate gemcitabine has been shown to only have a stable lifespan of 4 days determined by dynamic light scattering, before aggregation and drug release occurs [46]. this is a much shorter potential shelf life than the 4 weeks of high stability shown for the HNP-L-GEM.

***In vitro* evaluation**

The Mal-GEM released from the HNP is a prodrug. In order for gemcitabine to become liberated (for activity), the maleimide linker must be cleaved from the primary amine of gemcitabine. Such prodrugs are well documented [47]. In order for activity to be observed, the amide bond in the prodrug will be cleaved *via* hydrolysis, especially if taken up by endocytosis, or by enzymatic pathways.

The cytotoxic effect of GEM, HNP, Mal-GEM and the HNP-L-GEM formulation were observed in BxPC-3 cells over 72 h. Data from the MTT assays showed that the only compound exhibiting an IC_{50} value after 24 h was Mal-GEM (38 μg mL^{-1}) (SI-Table 1), whilst all the other compounds remained relatively non-toxic over the concentration ranges tested. The GEM and HNP-L-GEM did not exhibit IC_{50} values until after 48 h incubation (SI-Table1) with the lowest IC_{50} values observed after 72 h (Figure 5A). Data obtained from trypan blue exclusion is slightly different than that obtained from the MTT assay. Overall the IC_{50} values are lower when calculated *via* the MTT assay compared to the trypan blue exclusion assay. The main reason for this is that the MTT assay merely estimates the number of living cells based on their ability to metabolise MTT into formazan crystals and compares this activity to controls. The trypan blue exclusion assay will display a positive result for living cells, even if their metabolic processes have been reduced and hence, may give a better indication of actual cellular state. The data obtained using trypan blue exclusion consistently showed that no IC_{50} value was present after 24 h for all the particulates and drugs tested, with 50 % cell growth inhibition only observed after 48 h (SI-Table 1).

Overall the *in vitro* evaluation of Mal-GEM showed that that modification of the GEM molecule to include the linker had an impact on its overall toxicity. The IC_{50} of Mal-GEM after 48 h was 75 μg mL^{-1} (SI-Table 1) which was 4.3-fold higher than for GEM (17.5 μg mL^{-1}) which decreased to a 2.5–fold increase after 72 h (Figure 5B). However, after conjugation onto the HNP surface, the IC_{50} values observed after 48 h were comparable to that of the free GEM. This phenomenon, is not thought to be due to inherent toxicity of the HNPs, but due to the uptake mechanism of the drug/formulations. Figure 5C shows the cellular uptake in BxPC-3 cells measured up

to 24 h. In this study, GEM and Mal-GEM show similar intracellular drug levels at all time points which suggests that Mal-GEM enters the cell *via* similar mechanisms to the native drug molecule. It is likely that both the free drug and prodrug enter *via* the tight junction in the cell membrane which can be a time-consuming process, as well as being actively transported across the cell membrane with SLC28 and SLC29 nucleoside transporters [48,49]. Here it is clear to see, that after conjugation onto the nanoparticle surface a significant increase in cellular internalisation of drug is achieved ($P < 0.05$). Hence this would indicate that the cellular trafficking mechanism of the HNP-L-GEM is different compared with the drug and prodrug. Numerous studies have indicated that nanoparticulate vehicles enter cells *via* endocytosis. This is often relatively rapid and results in much higher intracellular concentrations. Hence, greater levels of drug are entering the cell which accounts for the IC_{50} decrease compared to the Mal-GEM.

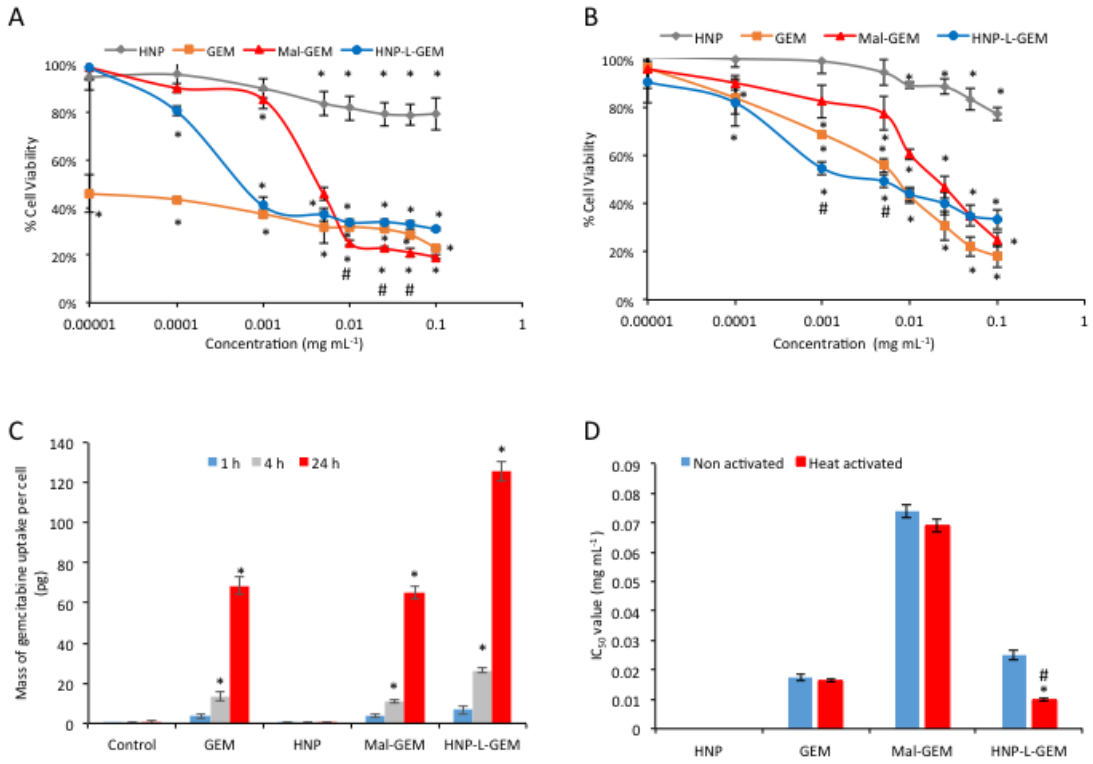

Figure 5. *In vitro cellular evaluation of the novel HNP-L-GEM formulation carried out on human pancreatic adenocarcinoma (BxPC-3) cells. Cytotoxicity measured by A) MTT assay and B) Trypan blue exclusion after 72 h exposure *denotes significance reduction in cell viability, # denotes significant reduction in viability compared to GEM ($p<0.01$). C) Cellular uptake of HNP-L-GEM at 1 h, 4 h and 24 h. *denotes significant increase compared with 1 h. D) Change in IC_{50} value after heat activation of HNP-L-GEM at 44 ºC for 30 min and incubation for 48 h measured via Trypan blue exclusion. *denotes significance reduction in IC_{50} compared with non-heat activated sample, # denotes significant reduction in viability compared to GEM ($p<0.01$). For all experiments ($n=3$, ±SD).*

It is acknowledged that all nanoparticle internalisation studies may contain some bias due to nanoparticles sticking to the cellular membrane externally being included within the analysis. This work uses reported assay in which each sample is washed multiple times before analysis in order to limit such bias [19]. In addition, due to the

final surface charge of the HNP-L-GEM (-2.6 mV) it is unlikely that they will stick onto the negatively charged cell membrane with great affinity and hence bias should be minimised.

The thermo-responsive nature of the HNP-L-GEM indicates that after heat activation (at 44 °C as determined *via* drug release) the immobilised Mal-GEM will be released from the surface of the HNP resulting in freely available drug to the cell. We postulated that this would result in a further increase in cytotoxic effect. Hence, a study was carried out which incubated the HNP-L-GEM with BxPC-3 cells for 24 h to ensure cellular uptake had occurred. The cells were then exposed to the elevated temperature of 44 °C for 0.5 h, before returning back to 37 °C for 24 h. The IC_{50} values both before and after heat activation are displayed in Figure 5D. As observed in the previous cytotoxicity studies, no IC_{50} was present for the HNPs. The GEM and Mal-GEM did not experience any significant change in their IC_{50} values after heat activation. However, the HNP-L-GEM experienced a 56 % increase in cytotoxicity after heating compared with no activation. This significant ($p<0.01$) reduction indicates that once heat activated the HNP-L-GEM undergoes retro Diels Alder reaction liberating Mal- GEM which results in a greater degree of toxicity compared to the immobilised inactivated HNP-L-GEM. This was expected as the rate of the retro Diels Alder reaction was shown to increase at increased temperatures. Additionally, the heat activated HNP-L-GEM resulted in a 26 % improvement in cytotoxicity compared to the free GEM.

Ideally the non-heat activated HNP-L-GEM would have remained non-toxic until heat activation had occurred. However, it is evident from the cell based assays that this is not the case. However, it may be possible to protect the drugs bound onto the surface of the HNPs using long chain polymers which will hinder the drug activity until liberated by heat.

Additional toxicity assays were carried out on the furan moiety (equivalent to those concentrations of gemcitabine reported) both before and after conjugation onto the HNP system at the specific binding concentration (SI-Figure 10). These studies showed, that there was no observable significant toxicity over 24 h and 48 h, with a slight toxic effect observed after 72 h. The biological toxicity from furans can be attributed to the metabolite: *Z*-2-butene-1,4-dial which contains two aldehyde functional groups in conjugation with a bridging C=C double bond. The conversion of furan into its metabolite form is catalysed by a cytochrome P450. In systemic circulation this may be problematic, especially in the liver. However, this formulation is being administered I.T., hence, two factors will contribute to the reduction of metabolism into the toxic form. These are: 1) there is a much-reduced presence of the catalyst enzyme P450 in pancreatic tumors and 2) the tumor microenvironment is hypoxic and hence probability of conversion is lower than would be for systemic metabolism. Currently, this is under study within our laboratories. Additionally, pancreatic tumors are extremely dense and solid and hence, leakage into systemic circulation is highly unlikely.

***In vivo* evaluation**

In vivo therapeutic studies were carried out in BxPC-3 xenograft tumors grown subcutaneous in nude mice. Before study commencement a dose toxicity study was carried out in healthy mice to ensure no gross toxicity would occur. These findings

(SI-Figure 11) showed that mice maintained their body weight and continued to grow over the study duration after administration of the HNPs and Mal-GEM.

Figure 6A shows the tumor volume measurements taken throughout the duration of the therapeutic study with the various treatment regimes. Those mice in the control and HNP groups both with and without laser irradiation did not last the duration of the study, due to their tumor volumes approaching the maximum humane limit as set out by the UK Home office. Figure 6B shows the excised tumors at the end of the study. In agreement with the tumor volume data it is observed that there is no significant difference in tumor size after HNP treatment (Figure 6B3) compared with the control (Figure 6B1). Likewise, there does not appear to be any effect on tumor volume or weight (Figure 6C) resulting from laser irradiation which can be observed in the control group with PBS treatment Figure 6B1&2 and also after HNP treatment (Figure 6B3&4).

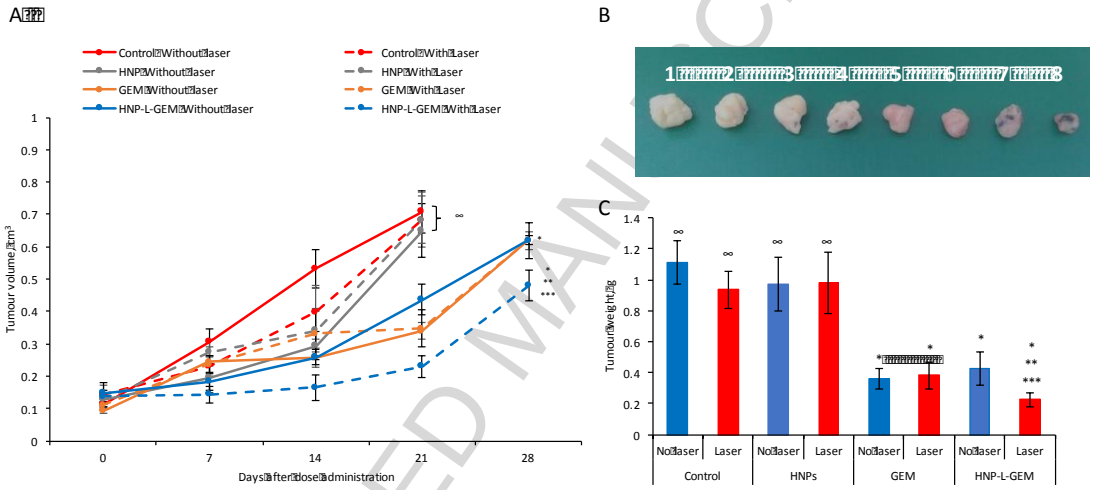

Figure 6. *In vivo evaluation on BxPC-3 xenograft models in Nu/Nu female mice (4-6 weeks old) dosed once a week at 3 mgKg^{-1} for 4 weeks. A) Comparison of tumor volume over study duration ∞ Study stopped before completion due to tumor volume approaching maximum humane volume (0.9 cm^3). B) Comparison of tumors after excision: 1) control, 2) control with laser irradiation, 3) HNP, 4) HNP with laser irradiation, 5) GEM, 6) GEM with laser irradiation, 7) HNP-L-GEM, 8) HNP-L-GEM with laser irradiation. Where laser irradiation was required this was carried out 24 h after dosing under anaesthetic. The tumor was irradiated at 1064 nm as for 20 sec using a ML-LASER-YB5 Q-switched Nd:YAG Laser Treatment System. Pulse width: 10 ns, pulse repetition frequency: 6 Hz, laser spot diameter: 3 mm, cooling system: water cooled with airflow cooling. The beam was collimated through concave lenses to a 1 mm diameter. C) Comparison of tumor weight after excision * denotes significance compared to controls, ** denotes significance compared to GEM, *** denotes significance compared to HNP-L-GEM without laser irradiation ($p<0.01$) ($n=5$, ±SE).*

As expected, those mice treated with GEM did experience significant tumor retardation ($p<0.01$) compared to the control groups as evident in the tumor volume and weight measurements (Figure 6). Again, the irradiation for 20 sec at 1064 nm did not have any impact on the tumor growth. Those mice treated with HNP-L-GEM did incur tumor retardation without laser irradiation. The tumors reduced in line with the GEM group with no significant increase or decrease in tumor weight or volume

observed. However, after laser irradiation a significant decrease in tumor volume (Figure 6A) and weight (Figure 6C) was observed, this was confirmed on excision of the tumors where it can clearly be seen that the tumors which underwent laser irradiation is visibly smaller than that of the non-irradiated group (Figure 6B). In fact, a 4.4–fold decrease in tumor weight compared to the control group and 1.6–fold decrease compared to the GEM was observed.

These exciting findings support the *in vitro* findings and indicate that once coupled onto the HNP it is likely that greater cellular internalisation of drug is occurring and that the retro Diels Alder reaction triggered by laser irradiation is liberating Mal-GEM which results in a greater effect compared to the GEM alone.

Conclusion

This study evaluates the use of linkages prepared by the Diels Alder reaction to reversibly bind gemcitabine onto the surface of HNPs for exploitation as a possible treatment in pancreatic cancer. This is the first report of a metallic nanoparticle delivery system for the transport and thermal release of GEM which utilizes chemical reactions rather than physical changes to elicit a controllable temperature dependant drug release. The novel formulation (HNP-L-GEM) produced was capable of high drug loading which appeared stable even upon reduction of pH. At elevated temperatures, the retro Diels Alder breakdown of the ligand occurred and resulted in rapid liberation of the prodrug. *In vitro* studies suggested that the prodrug itself was less toxic than free GEM, however after coupling onto the HNP rapid cellular internalisation occurred which resulted in 26 % reduction in cell viability compared with GEM after heat activation. The *in vivo* studies confirmed that heat activation of the HNP-L-GEM in BxPC-3 xenografts resulted in 62 % reduction in tumor weight compared with GEM.

These exciting results demonstrate the potential of the HNP-L-GEM formulation as a possible replacement to gemcitabine as a first line treatment for pancreatic cancer. However, in order for this formulation to be further optimised, further studies are being carried out to create to a second-generation system with addition of specific targeting peptides in order to encourage preferential uptake into the cancerous cells whilst evading the fibroblast cells. Furthermore, the clinical potential of this platform is not limited to mono drug therapy or indeed pancreatic cancer treatment, it would be possible to offer combined treatment regimens using multiple prodrugs attached to the HNP surface for any diseased state requiring controllable release of drug molecules.

Acknowledgements

The authors wish to acknowledge the EPSRC UK National Mass Spectrometry Facility at Swansea University.

Competing Interests

The authors would like to state that they have no competing interests.

Funding

This research did not receive any specific grant from funding agencies in the public, commercial, or not-for-profit sectors.

References

1. Zhang, Y. *et al.* Study human pancreatic cancer in mice: how close are they? *Biochimica et biophysica acta*. **1835**, 110–8 (2013).
2. Liu, Q.-H. *et al.* Surviving cells after treatment with gemcitabine or 5-fluorouracil for the study of de novo resistance of pancreatic cancer. *Cancer Letters*. **314**, 119–125 (2012).
3. Tran, B. *et al.* Association between ultraviolet radiation, skin sun sensitivity and risk of pancreatic cancer. *Cancer Epidemiology*. **37**, 886–892 (2013).
4. Zhang, Y. *et al.* Study Human Pancreatic Cancer in Mice: How Close Are They? *Biochimica et biophysica acta*. **1835**, 110–118 (2013).
5. Al Shemaili, J. *et al.* Frondoside A enhances the antiproliferative effects of gemcitabine in pancreatic cancer. *European Journal of Cancer*. **50**, 1391–1398 (2014).
6. Malvezzi, M. *et al.*, European cancer mortality predictions for the year 2013. *Annals of oncology : official journal of the European Society for Medical Oncology / ESMO*. **24**, 792–800 (2013).
7. Maraveyas, A. *et al.* Gemcitabine versus gemcitabine plus dalteparin thromboprophylaxis in pancreatic cancer. *European Journal of Cancer*. **48**, 1283–1292 (2012).
8. Zhang, G.-N. *et al.* Combination of salinomycin and gemcitabine eliminates pancreatic cancer cells. *Cancer Letters*. **313**, 137–144 (2011).
9. Pinho, A. V., *et al.* Chronic pancreatitis: A path to pancreatic cancer. *Cancer Letters*. **345**, 203–209 (2014).
10. Bockhorn, M. *et al.* Borderline resectable pancreatic cancer: A consensus statement by the International Study Group of Pancreatic Surgery (ISGPS). *Surgery*. **155**, 977–988 (2014).
11. Ling, Q. *et al.* The diversity between pancreatic head and body/tail cancers: clinical parameters and in vitro models. *Hepatobiliary & Pancreatic Diseases International*. **12**, 480–487 (2013).
12. Kristensen, A. *et al.* Does chemotherapy improve health-related quality of life in advanced pancreatic cancer? A systematic review. *Critical Reviews in Oncology/Hematology*. **99**, 286–298 (2016).
13. Brown, K. *et al.* The synthesis of gemcitabine. *Carbohydrate Research*. **387**, 59–73 (2014).
14. Hoskins, C. *et al.* In Vitro and In Vivo Anticancer Activity of a Novel Nano-sized Formulation Based on Self-assembling Polymers Against Pancreatic Cancer. *Pharmaceutical Research*,. **27**, 2694–2703 (2010).
15. Burris, H.A. *et al.* Improvements in survival and clinical benefit with gemcitabine as first-line therapy for patients with advanced pancreas cancer: a randomized trial. *Journal of clinical oncology : official journal of the American Society of Clinical Oncology*. **15**, 2403–13 (1997).
16. Song, W. *et al.* Polypeptide-based combination of paclitaxel and cisplatin for enhanced chemotherapy efficacy and reduced side-effects. *Acta Biomaterialia*. **10**, 1392–1402 (2014).
17. Sadjadi, S.-A., *et al.* Gemcitabine induced hemolytic uremic syndrome. *The American journal of case reports*. **13**,.89–91 (2012).
18. Moses, M.A., *et al.* Advancing the field of drug delivery: taking aim at cancer. *Cancer Cell*. **4**, 337–341 (2003).
19. Malekigorji, M., *et al.* A Thermally triggered theranostics for pancreatic cancer therapy. *Nanoscale*. **9,** 12735 (2017).

20. Khare, V., *et al.* Synthesis and characterization of TPGS-gemcitabine prodrug micelles for pancreatic cancer therapy. *RSC Advances*. **6**, 60126-60137 (2016).
21. Barnett, C. *et al.* Poly(allylamine) magnetomicelles for image guided drug delivery. *Pharmaceutical Nanotechnology*. **1**, 224-238 (2013).
22. Hosoki, T. Dynamic CT of pancreatic tumors. *A. J. Roentgenology*. **140**, 959-965 (1983).
23. Sofuni, A., *et al.* Differential diagnosis of pancreatic tumors using ultrasound contrast imaging. *J. Gastroenterology*. **40**, 518-525 (2005).
24. Sugahara, K.N. *et al.* Tissue-penetrating delivery of compounds and nanopartciles into tumours. *Cancer Cell*. **16**, 510-520 (2009).
25. Barnett, C. *et al.* Effect of the hybrid composition on the physicochemical properties and morphology of iron oxide–gold nanoparticles. *Journal of Nanoparticle Research*. **14**, 1170 (2012).
26. Curtis. A.D.M., *et al.* Heat Dissipation of Hybrid Iron Oxide-Gold Nanoparticles in an Agar Phantom. *Journal of Nanotechnology and Nanomedicine*, **6**, 6 (2015).
27. Oluwasamni, A., *et al.* Potential Of Hybrid Iron Oxide-Gold Nanoparticles As Thermal Triggers For Pancreatic Cancer Therapy. RSC Advances. **6**, 95044-95054 (2016).
28. Barnett, C., *et al.* Physical stability, biocompatibility and potential use of hybrid iron oxide-gold nanoparticles as drug carriers. *Journal of Nanoparticle Research*. **15**, 1706 (2013).
29. Kansea-thasan, A., *et al.* Comparison of image guided intratumoral versus intravenous delivery of therapeutivd nanoparticles for th treatment of heaptocellular carcinoma. *JVIR*. **S142,** 328 (2017).
30. Bakker, R.C., *et al.* Intratumoral treatment with radioactive beta-emitting microparticles: a systemic review. *J.Radiat. Oncol.* 1-19 (2017).
31. Okarvi, S., *et al.* Compariosn of introtuoral versus intravenous delivery of 177Lu-labeled bombersin peptide for targeting of breast carcinoma. *J. Nuc. Med.* **1**, 1349 (2016).
32. Hadja, J., *et al.* A non-controlled, single arm, open label, phase II study if intravenous and intratumoral administration of ParvOryx in patients with metastatic, inoperable pancreatic cancerL ParvOryx02 protocol. *BMC Cancer*. **17**, 576 (2017).
33. Manthe, R.L., *et al.* Tumor abalation and nanotechnology. *Mol. Pharm*. **7**, 1880-1898 (2010).
34. Li, C. A targted approach to cancer imaging and therapy. *Nat. Mater.* 1**3**, 110-115 (2014).
35. Song, H.Y. *et al.* Practical synthesis of maleimides and coumarin-linked probes for protein and antibody labelling via reduction of native disulfides. *Organic & Biomolecular Chemistry*. **7**, 3400 (2009).
36. Guo, Z., *et al.* Selective Protection of 2‘,2‘-Difluorodeoxycytidine (Gemcitabine). *The Journal of Organic Chemistry*. **64**, 8319–8322 (1999).
37. Temperini, A. *et al.* A simple acylation of thiols with anhydrides. *Tetrahedron Letters*. **51**, 5368-5371 (2010).
38. Hoskins, C. *et al.* Hybrid gold-iron oxide nanoparticles as a multifunctional platform for biomedical application. *Journal of Nanobiotechnology*. **10**, 27 (2012).
39. Fang, Y. *et al.* Enhanced cellular uptake and intracellular drug controlled release of VESylated gemcitabine prodrug nanocapsules. *Colloids and Surfaces B: Biointerfaces*. **128**, 357–362 (2015).

40. Banerjee, J., *et al.* Chronic nicotine inhibits the therapeutic effects of gemcitabine on pancreatic cancer *in vitro* and in mouse xenografts. *European Journal of Cancer*. **49**, 1152–1158 (2013).
41. Workman, P. *et al.* Guidelines for the welfare and use of animals in cancer research, *British Journal of Cancer*. **102**, 1555-1577 (2010).
42. Node, M. *et al.* Odorless substitutes for foul-smelling thiols: syntheses and applications. Tetrahedron Letters. **42**, 9207-9210 (2001).
43. Gregoritza, M., *et al.* The diela-alder reaction: a powerful tool for the design of drug delivery systems and biomaterials. *Eur. J. Pharm. Biopharm*. **97**, 438-453 (2015).
44. Shi, M., *et al.* Doxorubicin-conjugated immune-nanoparticles for intracellular anticancer drug delivery. *Adv. Funct. Mater.* **19**, 1689-1696 (2009).
45. Froidevaux, V., *et al.* Study of the Diels–Alder and retro-Diels–Alder reaction between furan derivatives and maleimide for the creation of new materials. *RSC Adv*. **5**, 37742–37754, (2015).
46. Ferreira, R. V *et al.* Thermosensitive gemcitabine-magnetoliposomes for combined hyperthermia and chemotherapy. *Nanotechnology*. **27**, 85105 (2016).
47. Moysan, E., *et al.* Gemcitabine versus modified gemctiabine: a review of several promising chemical modifications. *Mol. Pharm*. **10**, 430-444 (2013).
48. Mini, E. *et al.* Cellular pharmacology of gemcitabine. *Annals of Oncology*. **17**, v7–v12 (2006).
49. Rudin, D. *et al.* Gemcitabine Cytotoxicity: Interaction of Efflux and Deamination. *Journal of drug metabolism & toxicology*. **2**, 1–10 (2011).

Graphical abstract